Calculation of DEP and EWOD Forces for Application in Digital Microfluidics

Patrick M. Young

Kamran Mohseni
e-mail: mohseni@colorado.edu

Department of Aerospace Engineering Sciences,
University of Colorado at Boulder,
Boulder, CO 80309

Two primary methods for electrostatically actuating microdroplets in channels currently exist: dielectrophoresis (DEP) for electrically insulating fluids and electrowetting on dielectric (EWOD) for conducting fluids. In each case, a transverse electric field is used to create an electrostatic pressure, giving rise to the transport of individual liquid slugs. This paper examines the nature of the force distribution for both EWOD and DEP actuated droplets. The effects of system parameters such as contact angle and electrode length on the shape of the force density and its net integral are considered. A comparison of the scaling properties of DEP and EWOD for applications in digital microfluidics is presented. The net DEP force is shown to be strongly peaked when a droplet interface is located near the edge of a charged electrode and reduces to the well-known lumped parameter model in the appropriate limits. The effect of electrode spacing is seen to have an inversely proportional effect on the force experienced by the droplet, and the effect of increasing droplet contact angle is observed to increase the net force on the droplet.
[DOI: 10.1115/1.2956606]

1 Introduction

The field of digital microfluidics, in which discrete droplets are manipulated in place of continuous flows, has seen rapid development over the past few years for a variety of applications, from engineering to the life sciences [1–7], including variable focus lenses, display technology, fiber optics, and lab-on-a-chip devices. In particular, efficient and cost-effective lab-on-a-chip devices are in great demand, as they allow for highly repetitive laboratory tasks to become automated with the introduction of miniaturized and integrated systems [8]. This technique typically makes use of forces possessing favorable scaling relationships; prevalent examples include thermal or chemical surface tension modulation, electrowetting, and dielectrophoresis (DEP). In our group, digital microfluidics has been employed for active thermal management of compact electronic devices [9–11], design of a zero leakage microvalve [12], investigation of droplet morphology under electrowetting actuation [13], and design of an electrowetting microlense [14].

Accurate descriptions of actuation forces and resultant droplet velocities must be available when designing an integrated device making use of discretized flows. Currently, the most promising methods of droplet actuation in microfluidic devices are electrowetting on dielectric (EWOD) for conductive droplets [15–17] and DEP for electrically insulating droplets [18–22], where in both cases droplets are transported by sweeping an applied voltage along a microchannel ahead of the droplet. Numerical modeling of the droplet dynamics for EWOD and DEP configurations has been done using approximations of the electrostatic effect [13,23], but incorporation of the electrostatic force density into a direct simulation of the fluid mechanics is desired. For an example of such a simulation, see Ref. [24]. This paper presents numerical results describing the forces in DEP and EWOD for a droplet of fixed geometry. The lumped parameter result for the net droplet force is stated for DEP, and then compared with the results from direct numerical simulation of electrostatic forces. An analysis of the lumped force acting on an EWOD droplet has previously been presented by our group and others [2,25,26]. Here we extend these results to DEP, investigate the net forces and force distributions in DEP actuation, and provide comparison with EWOD.

The primary difference between an EWOD and a DEP actuated droplet is the nature of the fluid and its effect on the electric field's penetration into the media, see Fig. 1 for the basic setup of EWOD and DEP. For EWOD, an electrically conducting droplet is placed in a dielectric-coated channel lined with electrodes. A given electrode is then activated, creating an electric field that induces a charge accumulation on the surface of the fluid. This charge accumulation allows for the creation of a net force on the droplet, drawing the droplet toward the actuated electrode. Investigation of the interface profile and electrostatic distribution in EWOD has been explored in several papers [27–29]. The charge distribution near the contact line was found analytically, giving rise to a force distribution that is clustered in a region near the contact line on the order of h, the thickness of the dielectric layer. The interface profile used in this paper is assumed circular and fixed for all time, so any dynamic response to the electric field is not included and is a topic of future research.

DEP differs from EWOD in that the liquid is insulating, charge does not accumulate on the surface, and the electric field penetrates into the liquid. It is well known that a dielectric material is drawn into the gap between the parallel plate of a charged capacitor [30]. This is a result of the nonuniform fringing field located at the edge of the capacitor, providing a force pointing toward its center [30,31]. As opposed to EWOD, the dielectrophoretic force can act over the droplet's front face or within the bulk of the fluid itself. Jones [20,21] has explored the close relationship between DEP and EWOD on a theoretical basis, but for direct simulation of EWOD and DEP flows including electrostatic effects, a clear description of the force distribution is required. The cases considered here are for a perfect conductor (EWOD) and a perfect insulator (DEP), but there exist many fluids that exhibit properties of both a conductor and a dielectric, namely, leaky dielectrics [32]. This will be the topic of a future publication.

2 Governing Equations

In the problems considered in this investigation, the focus is on droplet flow resulting from electrical forces. In many microfluidic

Contributed by the Fluids Engineering Division of ASME for publication in the JOURNAL OF FLUIDS ENGINEERING. Manuscript received June 19, 2007; final manuscript received December 21, 2007; published online July 30, 2008. Assoc. Editor: Dennis Siginer. Paper presented at the ASME Fluids Engineering Division Summer Meeting and Exhibition (FEDSM2007), San Diego, CA, July 30–August 2, 2007.

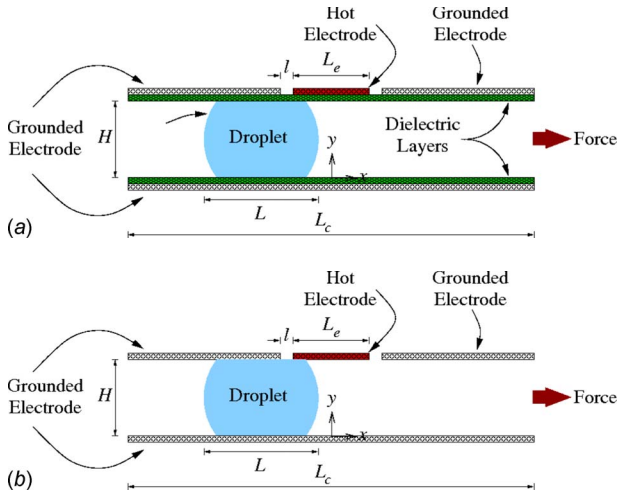

Fig. 1 The (*a*) EWOD and (*b*) DEP configurations. *H* is the droplet and the channel height and *L*, L_e, and L_c, are the droplet, the electrode, and the channel widths. *l* is the spacing between the hot and grounded electrodes.

applications, the dynamic currents are so small that the magnetic field can be ignored. In this situation, the governing equations for the electrical field are the electrostatic laws [33].

The governing equations of motion for incompressible fluids under electric effects are the mass, momentum, and electrostatic equations. Aside from the mechanical forces (pressure and shear stress), there exists Columbic forces due to any existing free charge as well as forces due to polarization. The corresponding boundary conditions at a fluid interface are obtained by integrating the mass and momentum equations through the interface.

The net effect of an applied electrical field on a given fluid is represented by an extra body force on the right hand side of the Navier–Stokes equations. The body force density $\mathbf{f_b}$ in a fluid resulting from the influence of an electric field can be written as

$$\mathbf{f_b} = \rho_f \mathbf{E} - \frac{1}{2}E^2\nabla\epsilon + \nabla\left(\frac{1}{2}\mathbf{E}\cdot\mathbf{E}\frac{\partial\epsilon}{\partial\rho}\right) \tag{1}$$

where ϵ is the fluid permittivity, ρ is the density of the fluid, ρ_f is the free electric charge density, and $\mathbf{E}$ is the electric field. This is the Korteweg–Helmholtz electric force density formulation [34–36]. The last term in this equation, the electrostriction force density term, can be ignored for incompressible flows. Hence, the body force density considered here is given by

$$\mathbf{f_b} = \rho_f \mathbf{E} - \tfrac{1}{2}E^2\nabla\epsilon \tag{2}$$

This force density provides a coupling between the droplet hydrodynamics and electric field. The first term of Eq. (2) is attributed to free charge in the system, while the second term is the contribution from the polarization of the medium.

The body force density (2) can be identically written as the divergence of a stress tensor, namely, the Maxwell stress tensor

$$\mathbf{f_b} = \nabla\cdot\mathbf{T}^M \tag{3}$$

or in tensorial notation

$$T_{ij}^M = \epsilon E_i E_j - \frac{\epsilon}{2}\delta_{ij}E_k E_k \tag{4}$$

This stress term accounts for both the forces due to the free electric charges and the forces due to the polarization of the material.

For a system consisting of perfectly insulating fluids (such as in DEP) with no free charge present, the first term in Eq. (2) can be disregarded. The second term in Eq. (2) is only nonzero at the interface between the two fluids, where there exists a gradient in ϵ. This indicates that the force density is located at the fluid interface, not distributed throughout the bulk of the fluid as the physical interpretation of the polarization effect indicates. The debate as to what point of view is correct is longstanding, but these seemingly contradictory interpretations of the body force density can be shown to be equivalent if care is taken [37]. The body force density due to the polarization forces is traditionally given by the Kelvin polarization body force density [38],

$$\mathbf{f_b} = (\mathbf{P}\cdot\nabla)\mathbf{E} = ((\epsilon-\epsilon_0)\mathbf{E}\cdot\nabla)\mathbf{E} = \epsilon\nabla\left(\frac{1}{2}E^2\right) - \nabla\left(\frac{\epsilon_0}{2}E^2\right) \tag{5}$$

where $\mathbf{P}=(\epsilon-\epsilon_0)\mathbf{E}$ is the polarization field. For an incompressible fluid, the scalar pressure only appears in the Navier–Stokes equations in terms of a gradient. The role of pressure is to ensure that continuity of the vector field is satisfied, and it takes on whatever value is needed to guarantee that this condition is always fulfilled. Hence, any other term that appears in the Navier–Stokes equations as the gradient of a scalar can be absorbed into the pressure [38]. This is true of the last term in Eq. (5), and so the effective body force density in view of the Kelvin representation is

$$\mathbf{f_b} = \epsilon\nabla\left(\tfrac{1}{2}E^2\right) \tag{6}$$

Now consider the Korteweg–Helmholtz formulation. Using the vector identity $\nabla(\phi\psi)=\phi\nabla\psi+\psi\nabla\phi$ and recalling that there is no free charge present in this system, Eq. (2) becomes

$$\mathbf{f_b} = \epsilon\nabla\left(\frac{1}{2}E^2\right) - \nabla\left(\frac{\epsilon}{2}E^2\right) \tag{7}$$

Since the last term in Eq. (7) is the gradient of a scalar, it can be absorbed into the pressure. Therefore, the difference in the Kelvin and Korteweg–Helmholtz body force densities is the gradient of a scalar, a term that has no dynamic significance for incompressible flows.

For a system where one fluid is significantly more conductive than the other (such as EWOD), the electric relaxation time for the conductive liquid can be assumed to be significantly shorter than the relevant hydrodynamic time scales. As a result, the interface can be regarded as a perfect conductor. For such a conductor under the influence of an electric field, all free charge in the system accumulates on the surface of the droplet. For such a setup, the force density is given by the first term in Eq. (2), except that for an ideal conductor we have $\rho_f \to \sigma_f$, where σ_f is the surface charge density. Note that this is no longer a body force density; it is confined to the surface of the droplet. The surface charge density can be rewritten using Gauss' law and the field itself is expressed as the average electric field intensity at the surface. Applying these two conditions and recalling that the electric field is always normal to the surface of a conductor gives the surface force density $\mathbf{f_s}$ at the interface,

$$\mathbf{f_s} = \sigma_f\mathbf{E} = \frac{\epsilon_{\text{ext}}}{2}E^2 \tag{8}$$

where ϵ_{ext} refers to the dielectric constant of the fluid external to the conductive droplet [39].

Thus, the difference in the force distribution for dielectric and conductive fluids is that of a body force density as opposed to a surface force density. This is an essential difference in regard to a numerical implementation of these forces coupled with the fluid equations.

The investigation of the electric force acting on droplets that are perfectly conductive and perfectly insulating is now considered in detail. The following introduces the nondimensionalization of the system considered in this paper.

2.1 Nondimensionalization. Figure 1 shows the setup for both the EWOD and DEP systems considered in this paper. Let the primes denote the nondimensionalized variables and set

$$x' = \frac{x}{H}, \quad y' = \frac{y}{H}, \quad V' = \frac{V}{V_0}, \quad \epsilon' = \frac{\epsilon}{\epsilon_0} \tag{9}$$

where H is the channel height, V_0 is the charged electrode voltage, and ϵ_0 is the electric permittivity of free space. This nomenclature is used to nondimensionalize the governing equations.

2.1.1 DEP. In electrostatics, $\mathbf{E}=-\nabla\mathbf{V}$ defines the relationship between the electric field $\mathbf{E}$ and the electric potential V. Using the potential formulation, Gauss' law reads

$$\nabla \cdot (\epsilon \nabla V) = \epsilon\left(\frac{\partial^2 V}{\partial x^2} + \frac{\partial^2 V}{\partial y^2}\right) + \frac{\partial \epsilon}{\partial x}\frac{\partial V}{\partial x} + \frac{\partial \epsilon}{\partial y}\frac{\partial V}{\partial y} = 0 \tag{10}$$

For the system considered in this paper, ϵ is a continuous function that takes on the value ϵ_{ext} outside the droplet, ϵ_{int} inside the droplet, and continuously transitions between ϵ_{ext} and ϵ_{int} linearly on the scale of the grid. Nondimensionalization of Eq. (10) gives

$$\epsilon'\left(\frac{\partial^2 V'}{\partial x'^2} + \frac{\partial^2 V'}{\partial y'^2}\right) + \frac{\partial \epsilon'}{\partial x'}\frac{\partial V'}{\partial x'} + \frac{\partial \epsilon'}{\partial y'}\frac{\partial V'}{\partial y'} = 0 \tag{11}$$

In the presence of the electric field, the atoms in a dielectric material polarize. The resulting dipoles experience a force from the electric field, and this electrostatic force density $\mathbf{f_b}$ of the electrically insulating droplet is given by Eq. (5). Equation (5) can then be integrated over the entire domain to give the net force acting on the insulating droplet. The relationship between the nondimensional body force density $\mathbf{f_b'}$ and the dimensional body force density $\mathbf{f_b}$ is

$$\mathbf{f_b} = \frac{\epsilon_0 V_0^2}{H^3}\mathbf{f_b'}$$

2.1.2 EWOD. In EWOD, the droplet is a conductor and hence there is no electric field present internally. Therefore, Eq. (10) reduces to Laplace's equation,

$$\frac{\partial^2 V'}{\partial x'^2} + \frac{\partial^2 V'}{\partial y'^2} = 0$$

with the appropriate boundary conditions.

The charge distribution resulting from the electric field present on the conducting droplet feels a force from the external electric field, giving rise to an electrostatic force always felt normal to the surface, given by Eq. (8). The integration of this force density gives the net force on the conductive droplet. The relationship between the nondimensional surface force density $\mathbf{f_s'}$ and the dimensional surface force density $\mathbf{f_s}$ for the EWOD configuration considered here is

$$\mathbf{f_s} = \frac{\epsilon_0 V_0^2}{H^2}\mathbf{f_s'}$$

The use of the primes has been dropped in the remainder of this paper for notational clarity.

2.2 Lumped Forced Calculations. The next two sections pertain to the forces at work in DEP and EWOD. The *total* force per unit area experienced by a droplet can be directly derived from capacitive energy considerations [30,31]. Differentiation of the system energy U gives the net force F in the horizontal direction, per unit area,

$$F = \frac{dU}{dx}$$

This method is demonstrated for both EWOD and DEP droplets in the section below. To calculate force *distributions*, numerical methods must be utilized, and this is presented in Sec. 3.

2.3 Lumped EWOD Force. Under EWOD actuation, the droplet is a conductor, and so all the charge is located at the fluid interface. Hence, the droplet experiences a surface force near its front and rear contact lines. We consider here only the case of a continuously grounded electrode, with the opposing side of the droplet in contact with a hot electrode with potential V on its advancing face and a grounded electrode on its receding face, as seen in Fig. 1(*a*). Ignoring the contributions of edge effects at the contact lines and the hot/cold electrode interface, the total capacitive energy in the system is

$$W = \frac{1}{2}c_l L V_{\text{drop}}^2 + \frac{1}{2}c_u\left(x + \frac{L}{2}\right)(V - V_{\text{drop}})^2 + \frac{1}{2}c_u\left(\frac{L}{2} - x\right)(-V_{\text{drop}})^2 \tag{12}$$

where c_u and c_l are the capacitances per unit area of the top and bottom dielectric coatings, V_{drop} is the voltage of the droplet, d is the thickness of the dielectric layers insulating the droplet from the electrode, and $x=0$ when the center of the droplet is directly under the left edge of the electrode. Assume $c_u=c_l=c=\epsilon_{\text{lay}}/d$, where ϵ_{lay} is the dielectric constant of the insulating layers. Then the droplet voltage is found by minimizing the total energy with respect to V_{drop}, giving a result of [36,39,40]

$$V_{\text{drop}} = \frac{V}{2}\left(\frac{x}{L} + \frac{1}{2}\right) \tag{13}$$

Adding Eq. (13) to Eq. (12) gives the system energy, which can be differentiated by x to give the net force in the horizontal direction,

$$F = \frac{dU}{dx} = \frac{\epsilon_{\text{lay}}}{4d}V^2\left(1 - \frac{2x}{L}\right) \tag{14}$$

Note that the total force on the droplet is a function of the droplet position with respect to the electrode. As a result, a droplet under EWOD actuation experiences a cyclic total force as it moves over a periodic array of electrodes. However, one should note that this lumped model breaks down when the droplet interfaces approach the electrode edges, as edge effects play an important role [26]. In such cases, one requires direct numerical simulation of the governing equations to obtain the net force, as described in Sec. 3.

2.4 Lumped DEP Force. Let ϵ_{int} and ϵ_{ext} be the dielectric constant of the droplet and the external fluid, respectively. Consider the system in Fig. 1(*b*) and recall that $x=0$ when the center of the droplet is directly under the left edge of the electrode in this section. The energy stored in the region where the droplet is under the charged electrode is given by $\frac{1}{2}c_{\text{int}}V^2$, where $c_{\text{int}}=\epsilon_{\text{int}}/H(x-L)V^2$ is the capacitance per unit area of this region. The energy stored in the region under the charged electrode where the droplet is *not* present is given by $\frac{1}{2}c_{\text{ext}}V^2$, where $c_{\text{ext}}=\epsilon_{\text{ext}}/H(L_e-x)V^2$ is the capacitance per unit area of this second region. Then the net force per unit area is given by

$$F = \frac{dU}{dx} = \frac{d}{dx}\left(\frac{1}{2}c_{\text{int}}V^2 + \frac{1}{2}c_{\text{ext}}V^2\right) = \frac{1}{2}\frac{\epsilon_{\text{int}} - \epsilon_{\text{ext}}}{H}V^2 \tag{15}$$

where ϵ_{int} is the dielectric constant of the fluid itself and ϵ_{ext} is the dielectric constant of the external fluid. This force is seen to be the difference in capacitive energy between a dielectric-filled channel and an empty channel. Again, this model is only valid when the droplet interfaces are well away from any fringing fields. Note that the droplet height, H, appears directly in this expression for F; this factor gives DEP a different scaling than EWOD [26,41]. The velocity of an EWOD droplet depends on H/L, where L is the length of the droplet. In contrast, the velocity of a dielectric droplet depends only on $1/L$, making DEP increasingly effective for very small channel sizes.

2.4.1 Maxwell Stress Tensor. The above lumped parameter analysis can equivalently be derived using the Maxwell stress tensor with a judicious choice of integration path [20]. However, the stress tensor calculation fails when the droplet interface is near the edge of the electrode.

First, consider the integration paths in Fig. 2(*a*). Here the drop-

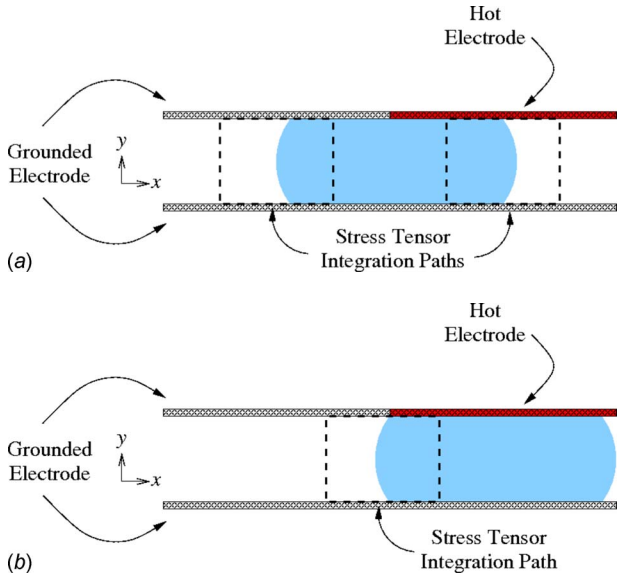

Fig. 2 Integration paths used when calculating the force with the Maxwell stress tensor when (*a*) the droplet interface is far away from the electrode interface and (*b*) when the droplet interface is near the electrode interface.

let interface is well away from the electrode interface. The vertical components of the integration path are assumed to be far enough away from regions of nonuniformity that **E** is known analytically. The contributions along the horizontal components of the integration path take the form (when only concerned with force in the horizontal direction)

$$\int T_{12} da = \int \epsilon E_1 E_2 da$$

where the subscripts 1 and 2 refer to the x and y directions, respectively. Since the horizontal components lie along the electrodes, $E_1=0$ and so these parts of the integration path contribute nothing to the stress tensor integration.

Now consider the integration path in Fig. 2(*b*). The droplet interface is now near the electrode interface, and the integration path must lie across the hot/cold electrode interface to ensure that the vertical components of the path are in regions where **E** is known analytically. Unfortunately, it can no longer be assumed that $E_1=0$ all along the upper horizontal path because of the discontinuity, and so the stress tensor method fails when droplet interfaces are near electrode interfaces. In order to calculate the net force in these regions, numerical methods need to be utilized.

Note that the same problem persists even when a gap is added between the hot and cold electrodes, as one would need to integrate around the corners of the electrode, where the normal direction is ambiguous.

3 Force Distribution

In this section, we present a detailed analysis of the electric force distribution of a droplet for both EWOD and DEP. The lumped analysis is only valid when the interface is far from the fringing fields. While the total force experienced by a droplet under EWOD and DEP was given in the previous section, a complete solution of the Navier–Stokes equations including electrohydrodynamic effects requires a detailed knowledge of the force distribution, as given below.

3.1 EWOD Force Distribution. Consider a droplet with no net charge while it is electrically isolated from the electrodes. Since no volumetric free charge exists in the solution region, the potential is found by solving Laplace's equation outside of the droplet with the appropriate boundary conditions[42]. The boundary condition on the surface of the conductor is

$$\sigma_f = -\epsilon_{\text{ext}} \frac{\partial V}{\partial n} \tag{16}$$

with the entire droplet itself held at a constant potential V_{drop}. The charge distribution and droplet potential are not in general known a priori and must be found as part of the numerical solution[43]. This is accomplished via a shooting method in which two initial guesses for the droplet voltage are assumed; the net charge on the surface is calculated by integrating $\sigma_f=-\epsilon_{\text{ext}}(\partial V/\partial n)$ over the boundary, and a subsequent guess for V_{drop} is calculated via the secant method. Convergence is reached when the integration of the surface charge is near enough to zero, specified by the user (a value of 10^{-6} was used in these calculations), see Ref. [26] for details.

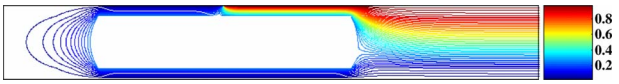

Fig. 3 Example calculation of the electric equipotentials surrounding a droplet in EWOD configuration; the contact angle is 10 deg. In nondimensional units, $h=1$, $L=2$, and the length of the computational domain=10. See Ref. [26] for more details.

The Laplace equation is discretized using second-order centered differences and the resulting system is solved iteratively. An example calculation of the electric potential around a conducting droplet is shown in Fig. 3. The droplet is centered over the voltage step, and the channel is lined with dielectric layers equal thicknesses given by $d=0.1H$. The contour lines are densely concentrated around the four corners of the droplet, indicating the outward pressure along both faces.

The charge distribution and force densities on the surfaces of a straight-sided centered droplet are shown in Fig. 4. On the rear interface, the distributions are symmetric about the centerline and always of the same sign. On the front of the droplet, the charge changes sign at a location given roughly by

$$y = \frac{V_{\text{drop}}}{V} H \tag{17}$$

and the force density is most strongly peaked near the hot electrode. Note that the force distributions are localized within a distance of order d near the droplet edges. In many EWOD applications, d is less than 1% of H, and the force is often treated as if it were a point force acting exactly at the contact line [27]. For more details on the numerical force calculation in EWOD including verification, see Ref. [26].

3.2 DEP Force Distribution. The simple bulk parameter analysis presented earlier for a dielectric medium is only valid for certain locations of the dielectric fluid slug relative to the actuating electrode. When the fluid interface is near a voltage jump, the form of the system energy will be strongly dependent on the exact location of the fluid. Equation (15) is therefore expected to be accurate only when the droplet is straddling the hot/cold electrode interface with its own faces reasonably far away. In addition, Eq. (15) does not address the force on a droplet approaching, but not yet in contact with, a voltage jump. To address these situations, numerical methods must be utilized.

To calculate the desired force density, we must first solve Eq. (10) numerically to obtain the electric field of the system. The net force on the droplet is an artifact of the increase in the gradient of the square of the electric field. If the interface is located in a region where the divergence of E^2, the contribution to the net body force of this region is greatly increased. Because of this, it is critically important that the electric field is accurately resolved

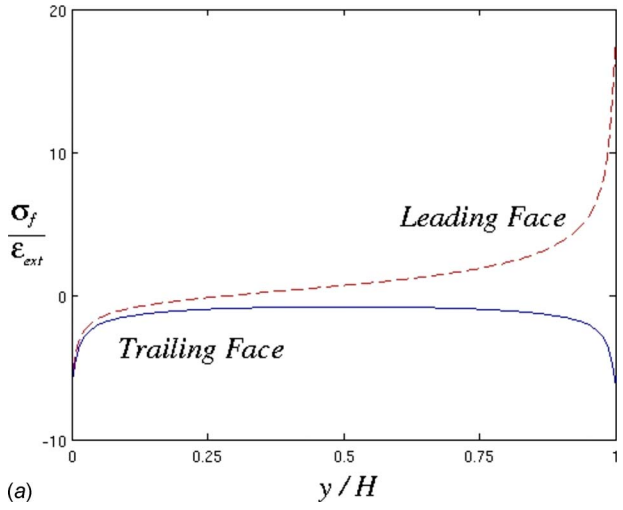

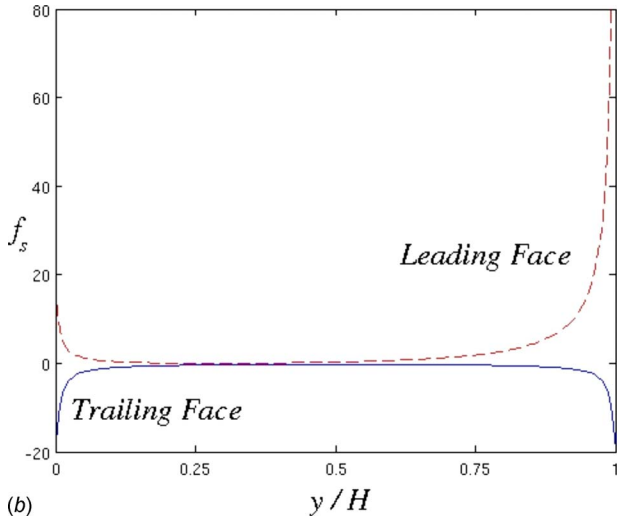

Fig. 4 Charge distributions (*a*) and force densities (*b*) on the leading and trailing interfaces of an EWOD-activated droplet. Contact angle is 0 deg. See Ref. [26] for more details.

near the fringing fields located at the edges of the electrodes. To achieve this resolution, a nonuniform grid is applied in the x-direction. Let x and x' denote the horizontal coordinate in the physical and computational planes, respectively. We define the relationship between the two planes as

$$x' = x_{\max}\left(A + \frac{1}{\beta_x}\sinh^{-1}\left(\left(\frac{x}{x_0} - 1\right)B\right)\right)$$

where

$$A = \frac{1}{2\beta_x}\log\left(\frac{1 + (e^{\beta_x} - 1)x_0/x_{\max}}{1 + (e^{-\beta_x} - 1)x_0/x_{\max}}\right)$$

$$B = \sinh(\beta_x A)$$

where $x_{\max}$ is the maximum value in the physical domain, x_0 is where we desire to cluster nodes, and β_x controls the amount of clustering about x_0, where greater values of β_x lead to a higher concentration of points about x_0 [44]. See Fig. 6 for schematics of the grid distribution in the computational domain.

Transforming Eq. (10) to the computational plane, we arrive at

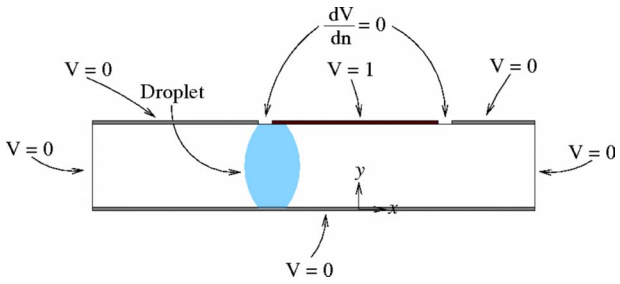

Fig. 5 Boundary conditions used in numerically solving for the electric potential surrounding a dielectric fluid in DEP configuration

$$\epsilon\left(\frac{\partial^2 V}{\partial x'^2}\left(\frac{\partial x'}{\partial x}\right)^2 + \frac{\partial V}{\partial x'}\frac{\partial^2 x'}{\partial x^2} + \frac{\partial^2 V}{\partial y^2}\right) + \frac{\partial \epsilon}{\partial x'}\frac{\partial V}{\partial x'}\left(\frac{\partial x'}{\partial x}\right)^2 + \frac{\partial \epsilon}{\partial y}\frac{\partial V}{\partial y} = 0 \tag{18}$$

where

$$\frac{\partial x'}{\partial x} = \frac{x_{\max}B}{\beta_x x_0((x/x_0 - 1)^2B^2 + 1)^{1/2}}$$

$$\frac{\partial^2 x'}{\partial x^2} = -\frac{x_{\max}B^3(x/x_0 - 1)}{\beta_x x_0^2((x/x_0 - 1)^2B^2 + 1)^{3/2}}$$

Each term in Eq. (18) is discretized using the standard second-order centered finite difference approximation. For a given node (i,j), the discretization of Eq. (18) yields the following relationship:

$$\begin{aligned}
&\frac{1}{(\Delta y)^2}\left(\epsilon_{i,j} - \frac{\epsilon_{i,j+1} - \epsilon_{i,j-1}}{4}\right)V_{i,j-1} + \left(\frac{\epsilon_{i,j}}{(\Delta x)^2}\left(\frac{\partial x'}{\partial x}\right)^2 - \frac{\epsilon_{i,j}}{2\Delta x}\frac{\partial^2 x'}{\partial x^2}\right.\\
&\quad\left. - \frac{\epsilon_{i+1,j} - \epsilon_{i-1,j}}{4(\Delta x)^2}\left(\frac{\partial x'}{\partial x}\right)^2\right)V_{i-1,j} - 2\epsilon_{i,j}\left(\frac{1}{(\Delta x)^2}\left(\frac{\partial x'}{\partial x}\right)^2\right.\\
&\quad\left. + \frac{1}{(\Delta y)^2}\right)V_{i,j} + \left(\frac{\epsilon_{i,j}}{(\Delta x)^2}\left(\frac{\partial x'}{\partial x}\right)^2 + \frac{\epsilon_{i,j}}{2\Delta x}\frac{\partial^2 x'}{\partial x^2}\right.\\
&\quad\left. + \frac{\epsilon_{i+1,j} - \epsilon_{i-1,j}}{4(\Delta x)^2}\left(\frac{\partial x'}{\partial x}\right)^2\right)V_{i+1,j} + \frac{1}{(\Delta y)^2}\left(\epsilon_{i,j}\right.\\
&\quad\left. + \frac{\epsilon_{i,j+1} - \epsilon_{i,j-1}}{4}\right)V_{i,j+1} = 0
\end{aligned}$$

The domain in Fig. 5 is discretized using this formula, and the resulting matrix equation is then solved using iterative methods. For the gap between the hot and cold electrodes, the boundary condition $\partial V/\partial n = 0$, where n designates the normal direction, is applied.

Recall that the electrostatic force density is given by Eq. (6). To find the net force on a fluid slug, it is necessary to integrate Eq. (6) all along the channel, not just over the volume of droplet itself. This is because the fringing fields at the edge of the charged capacitor exert an inward force on whatever material is present, including the external fluid surrounding the droplet; this force is felt as a pressure on the droplet interfaces, and the flow proceeds

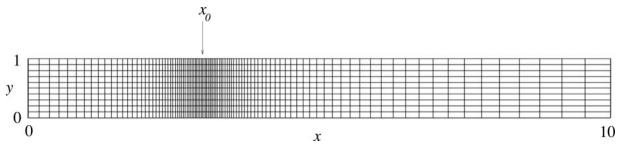

Fig. 6 Representative grid used in computation; not all computational nodes are shown. x_0 is the point of maximum clustering.

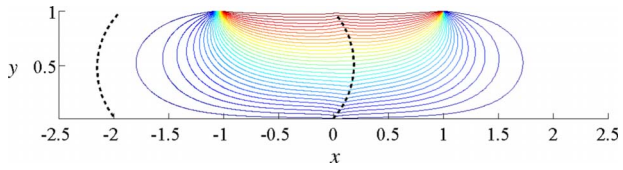

Fig. 7 Example calculation of the electric potential *V* for a droplet centered under the left edge of an electrode

such that the material with greatest electric permittivity is drawn into the "hot" capacitive region. The force on a droplet thus changes sign as it moves over a charged electrode. In addition, the DEP force becomes repulsive for droplets immersed in a fluid of higher dielectric permittivity. Note that, for completeness, in this paper we consider the full, symmetric case of a droplet moving into and out of a capacitor, resulting in antisymmetric force peaks on the fluid. Therefore, it is recommended that the electrodes in a DEP device be narrower than the droplet's length, and that they be actuated so that a fluid slug is pulled forward with a force always of the same sign.

The nondimensionalized values used in the following computations are $H=1$, $L=2$, $L_c=10$, $L_e=2$, $\epsilon_{ext}=1$, and $\epsilon_{int}=3$, unless otherwise stated. Generally 2001 nodes were used in the horizontal direction with $B_x=2$ and x_0 located at the leading edge of the droplet, and 51 nodes were used in the vertical direction unless otherwise specified. Figure 7 shows an example calculation of the electric potential for a droplet centered underneath the left edge of the electrode. The electric field is found by taking the gradient of this potential and the electrostatic force density is then found by squaring the electric field and again taking the gradient. As a consequence, the force density is very strongly localized in regions where the potential gradient is largest, i.e., near the hot/cold electrode interface.

To ensure that the resolution is high enough to capture the behavior of the net force, the force was calculated as the droplet moved over the edge of the electrode. The convergence of the method for a varied number of points in the horizontal direction is seen in Fig. 8. Note that capturing the height of the peak requires more resolution than nearby values of the total force.

Figure 9(*a*) shows the net force experienced by the droplet as a function of position. The gap width between the hot and cold electrodes is set to 2.5% of H. A sharp spike in force as the droplet approaches the electrode can be seen. Once the leading droplet edge has passed underneath the electrode, the force experienced by the droplet approaches a net nondimensionalized force of 1, which agrees with the theoretical result (15) from the lumped force calculation. As the droplet continues to move, it experiences a strong *increase* in force to the right as the leading edge of the droplet approaches the far edge of the electrode. It is at this point that one would want to activate the next electrode in the series to keep the droplet moving to the right. This force is counteracted as the leading edge exits the region covered by the hot electrode and the behavior described above is repeated but in the opposite direction.

Figures 9(*b*) and 9(*c*) show a similar force plot but with wider electrodes so that the active electrode is longer than the entire length of the droplet. In this case, we observe a *decrease* in net

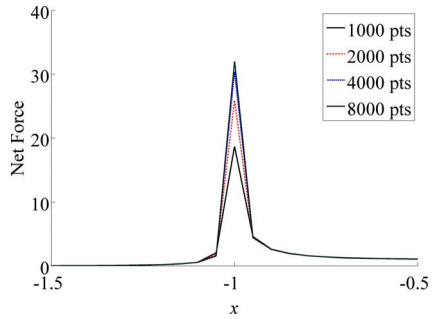

Fig. 8 Convergence of force calculation as resolution increases. The number of points is in terms of the discretization in the *x*-direction.

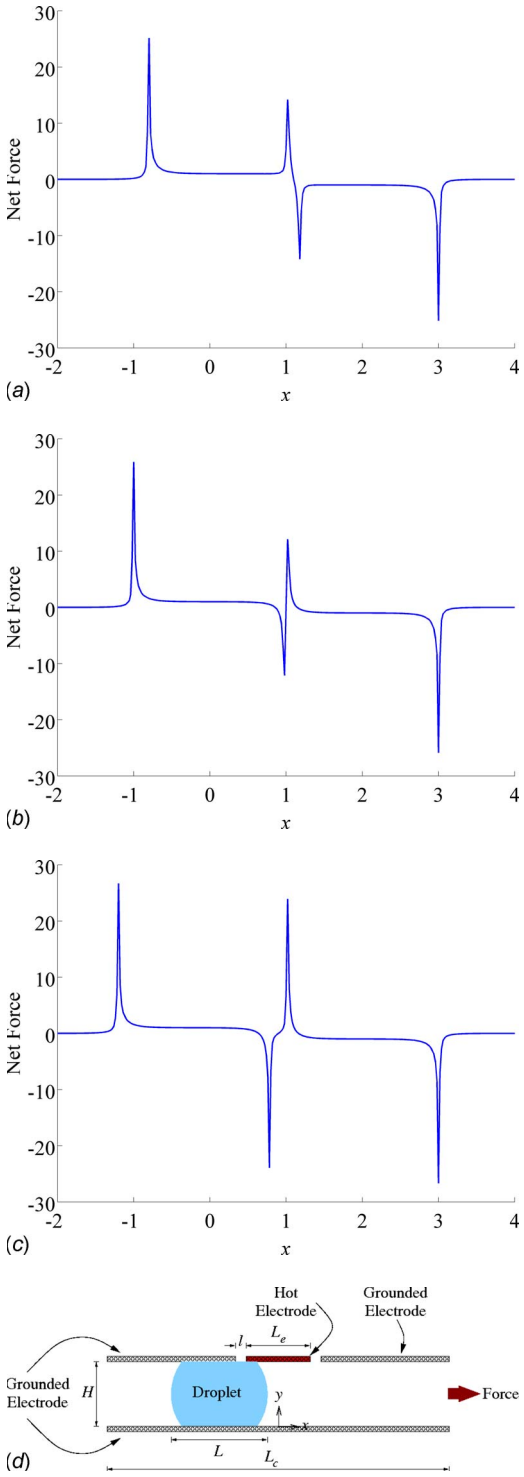

Fig. 9 The net horizontal force experienced by the droplet as a function of position. Position is given by the location of the center of the droplet with respect to the center of the electrode. (*a*) $L_e=1.8$ and $L=2.0$; (*b*) $L_e=2.0$ and $L=2.0$; (*c*) $L_e=2.2$ and $L=2.0$; and (*d*) setup for force calculations in (*a*)–(*c*).

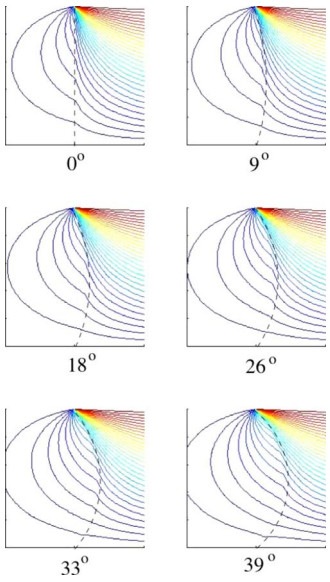

Fig. 10 Electric potential for various contact angles. The increased gradient from the curvature results in greater net horizontal force.

force as the leading droplet edge approaches the right edge of the active electrode. Because the electrode is longer than the droplet, the trailing edge of the droplet experiences a negative force as it nears the left edge of the electrode, causing the force to be directed to the left. This occurs before the leading edge of the droplet is near the right edge of the electrode, as in Fig. 9(*a*). This situation is not ideal if one hopes to use a sequence of electrodes to transport the droplet to the right. Clearly, a smaller electrode is desirable in applications. This phenomenon demonstrates how the use of narrow electrodes and the importance of accurate electrode actuation is critical in DEP to avoid "stalling" the droplet in the channel.

The spikes in force seen in Figures 9(*a*)–9(*c*) can be explained by the drastic change in the gradient of the electric field when the droplet edge (and hence the dielectric medium) passes through the fringing field induced by the electrodes. The effect of droplet contact angle can enhance this effect, see Figs. 10 and 11, increasing the net force on the droplet while it is in this region. This effect will only be seen when the droplet interface is located near the fringing field; otherwise the net force can be obtained by the previously mentioned analytical results. This is a result of the interface physically extending farther into the domain when the contact angle is increased; the nonuniformity of the fringing field gives rise to the increase in force as the interface extends further into the region.

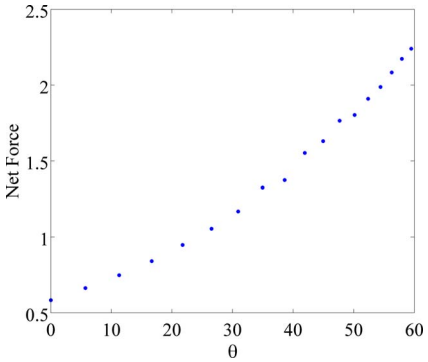

Fig. 11 Increase in net horizontal force as the contact angle θ increases for a droplet with the leading edge placed near the left edge of the electrode near the fringing field

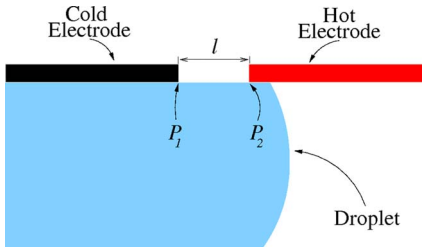

Fig. 12 DEP configuration. The gap between the adjacent electrodes is *l*.

The scaling in DEP varies with L, when the droplet interfaces are well removed from the electrode edges. However, when the interfaces are near the edges of the electrode, the force scaling is dependent on l, the distance between the hot and cold electrodes, as seen in Fig. 12. In EWOD, a surface force density is distributed over the droplet's front and rear interfaces and is localized within a length scale equal to the thickness of the dielectric layers lining the channel. DEP differs from EWOD in that a volumetric force density is localized within a radius on the order of the gap between the hot and cold electrodes. While varying the electrode gap width does not affect the net force when the droplet interfaces are sufficiently far from the voltage jump, it does spread the force distribution over a larger area.

Figure 13(*a*) shows the decrease in total force on the droplet as l increases. As the leading edge of the droplet approaches the electrode, the net force felt by the droplet begins to grow. The rise in force occurs over the same distance as l, resulting in a broadening of the peak as l increases and a reduction in maximum force obtained. Reducing the magnitude of the force by increasing the gap width of the electrodes may be beneficial in applications, as strong electric fields can cause local dielectric breakdown of the fluid.

Scaling these peaks with respect to the gap width demonstrates the linearity of the relationship. We see the same characteristic features of the peaks align when scaled in this manner, as seen in

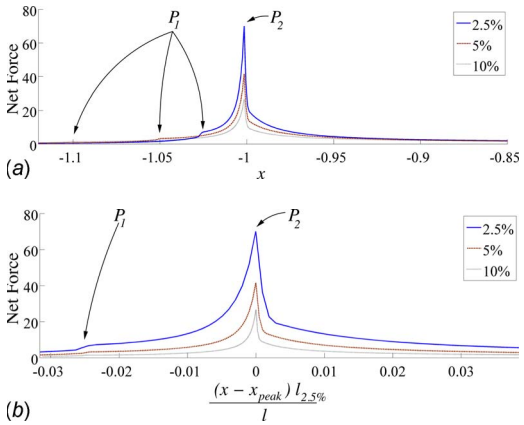

Fig. 13 Net horizontal force versus *x*, for various values of *l*. The percentage shown indicates the width of the gap with respect to *H*. P_1 and P_2 are the same, as shown in Fig. 12. (*a*) Force versus position. $x=-1$ when the leading edge of the droplet is flush with the edge of the electrode. (*b*) Net horizontal force versus nondimensional position (relative to the length of the gap between the electrodes). $l_{2.5\%}$ is the length of the gap for $l=0.025H$ and x_{peak} is the location of the maximum net force.

Fig. 13(*b*). This is a beneficial relationship for the fabrication of microfluidic devices, as the behavior of droplets with different gap scalings can be extrapolated from known data.

Note that the net forces calculated in this paper pertain to a solid as well as a liquid; the dynamics of the medium do not play a role in these calculations. To fully integrate the electrostatics into a fluid solver, the force density (2) resulting from the electric field can be added as a body force acting upon the fluid. Investigation into fluid solvers coupled with the electrostatic effect is beginning to occur, for example, see Ref. [24]. Besides the bulk transport of the droplet, it is expected that some interesting dynamics would arise from adding the force distribution into a fluid solver. For instance, consider a droplet centered over the edge of a hot electrode, as seen in Fig 7. The droplet experiences a net force pulling it into the region of the hot electrode resulting from nonuniformity of the field. The field is particularly nonuniform in the region of the droplet located near the gap separating the hot and cold electrodes (i.e., the points P_1 and P_2 seen in Fig. 12). This region contains two peaks of extremely large magnitude but opposite signs. The net effect from this region is canceled out in the integration of the force density, but one would expect the fluid to respond to these peaks locally, creating some local fluid circulation. Furthermore, the net force is only in the horizontal direction, but forces are present in the vertical direction as well, which certainly will change the shape of the droplet.

4 Conclusion

The two primary methods for droplet transport in digital microfluidics, namely, DEP and EWOD have been investigated. EWOD works with conductive fluids while DEP pertains to insulating fluids. In both cases, droplet transport is achieved by sweeping a voltage along a microchannel ahead of the droplet. A review of the Korteweg–Helmholtz and Kelvin force density formulations has been given as well as how these force densities apply to DEP and EWOD.

An energy minimization approach was used to calculate the total force acting on a droplet under EWOD and DEP actuation. It is seen that the total force for EWOD scales as $1/d$, where d is the dielectric layer thickness, while for DEP the total force scales as $1/H$, where H is the channel height, which leads to different velocity scalings of H/L and $1/L$ for EWOD and DEP, respectively. This indicates that DEP will be increasingly effective for small channel heights.

Investigation of the force distributions for EWOD shows how the force density is confined to the surface of the droplet while in DEP it is spread throughout the bulk. This is a critical difference to note when implementing any computational simulation of EWOD and DEP. Two methods were demonstrated for numerically calculating the force distribution for EWOD and DEP. To fully resolve the force when interfaces are located near regions of nonuniformity in the electric field, greater resolution is required. In DEP, it is noted that interface curvature can enhance the net force experienced by the droplet as a result of the fluid interface extending further into the electric field. When a droplet is under DEP actuation, small electrode sizes in comparison to droplet length are preferable, as they keep the net force pointing in the same direction as the droplet moves under the electrode and avoiding any possible stalling of the droplet in the channel. Investigation of the gap width l between electrodes demonstrates how DEP scales with respect to l. As the interface travels through the region represented by l, the net force acting on the droplet increases. A decrease in the maximum force obtained also occurs as l grows. In engineering applications, this parameter could be used to lessen the magnitude of the force if dielectric breakdown of the fluid was a concern.

Acknowledgment

The authors would like to acknowledge partial funding from the Defense Advanced Research Projects Agency (DARPA) and the National Science Foundation (NSF). The authors benefited from discussions with Mr. E. Baird.

References

[1] Cho, S. K., Moon, H., and Kim, C. J., 2003, "Creating, Transporting, Cutting, and Merging Liquid Droplets by Electrowetting-Based Actuation for Digital Microfluidic Circuits," J. Microelectromech. Syst., **12**(1), pp. 70–80.

[2] Cooney, C. G., Chen, C.-Y., Nadim, A., and Sterling, J. D., 2006, "Electrowetting Droplet Microfluidics on a Single Planar Surface," Microfluid. Nanofluid., **2**(5), pp. 435–446.

[3] Lee, J., Moon, H., Fowler, J., Kim, C. J., and Schoellhammer, T., 2001, "Addressable Micro Liquid Handling by Electric Control Of Surface Tension," *Proceedings of the IEEE International Conference MEMS*, Interlaken, Switzerland, Jan., pp. 499–502.

[4] Pollack, M. G., Fair, R. B., and Shenderov, A. D., 2000, "Electrowetting-Based Actuation of Liquid Droplets for Microfluidic Applications," Appl. Phys. Lett., **77**(11), pp. 1725–1726.

[5] Pollack, M. G., Shenderov, A. D., and Fair, R. B., 2002, "Electrowetting-Based Actuation of Droplets for Integrated Microfluidics," Lab Chip, **2**(2), pp. 96–101.

[6] Shapiro, B., Moon, H., Garrell, R. L., and Kim, C. J., 2003, "Equilibrium Behavior of Sessile Drops Under Surface Tension, Applied External Fields, and Material Variations," J. Appl. Phys., **93**(9), pp. 5794–5811.

[7] Wang, K. L., and Jones, T. B., 2005, "Electrowetting Dynamics of Microfluidic Actuation," Langmuir, **21**, pp. 4211–4217.

[8] Charkrabarty, K., and Zeng, J., 2006, *Design Automation Methods and Tools for Microfluidics-Based Biochips*, Springer, New York.

[9] Baird, E., and Mohseni, K., 2008, "Digitized Heat Transfer: A New Paradigm for Thermal Management of Compact Micro-Systems," IEEE Trans. Compon. Packag. Technol., **31**(1), pp. 143–151.

[10] Mohseni, K., 2005, "Effective Cooling of Integrated Circuits Using Liquid Alloy Electrowetting," *Proceedings of the Semiconductor Thermal Measurement, Modeling, and Management Symposium (SEMI-Therm)*, San Jose, CA, Mar. 15–17. IEEE.

[11] Mohseni, K., and Baird, E., 2007, "Digitized Heat Transfer Using Electrowetting on Dielectric," Nanoscale Microscale Thermophys. Eng., **11**(1&2), pp. 99–108.

[12] Mohseni, K., and Dolatabadi, A., 2006, "An Electrowetting Microvalve: Numerical Simulation," Ann. N.Y. Acad. Sci., **1077**(1), pp. 415–425.

[13] Dolatabadi, A., Mohseni, K., and Arzpeyma, A., 2006, "Behaviour of a Moving Droplet Under Electrowetting Actuation, Numerical Simulation," Can. J. Chem. Eng., **84**(1), pp. 17–21.

[14] Chang, Y.-J., Mohseni, K., and Bright, V., 2007, "Fabrication of Tapered SU-8 Structure and Effect of Sidewall Angle for a Variable Focus Microlens Using EWOD," Sens. Actuators, A, **136**(2), pp. 546–553.

[15] Cho, S. K., Fan, S. K., Moon, H., and Kim, C. J., 2002, "Towards Digital Microfluidic Circuits: Creating, Transporting, Cutting, and Merging Liquid Droplets by Electrowetting-Based Actuation," in *Technical Digest. MEMS, Proceedings 15th IEEE International Conference MEMS*, pp. 32–35.

[16] Fair, R. B., Srinivasan, V., Ren, H., Paik, P., and Pollack, M. G., 2003, "Electrowetting-Based On-Chip Sample Processing for Integrated Microfluidics," Tech. Dig. - Int. Electron Devices Meet., **2003**, pp. 32.5.1–32.5.4.

[17] Moon, H., Cho, S. K., Garrell, R., and Kim, C. J., 2002, "Low Voltage Electrowetting-On-Dielectric," J. Appl. Phys., **92**(7), pp. 4080–4087.

[18] Deval, J., Tabeling, P., and Ho, C. M., 2002, "A Dielectrophoretic Chaotic Mixer," *15th IEEE International Conference on MEMS (MEMS 2002)*, Las Vegas, NV, pp. 36–39.

[19] Gascoyne, P. R. C., Vykoukal, J. V., Schwartz, J. A., Anderson, T. J., Vykoukal, D. M., Current, K. W., McConaghy, C., Becker, F. F., and Andrews, C., 2004, "Dielectrophoresis-Based Programmable Fluidic Processors," Lab Chip, **4**(4), pp. 299–309.

[20] Jones, T. B., 2002, "On the Relationship of Dielectrophoresis and Electrowetting," Langmuir, **18**, pp. 4437–4443.

[21] Jones, T. B., Fowler, J. D., Chang, Y. S., and Kim, C. J., 2003, "Frequency-Based Relationship of Electrowetting and Dielectrophoretic Liquid Microactuation," Langmuir, **19**, pp. 7646–7651.

[22] Jones, T. B., and Wang, K. L., 2004, "Frequency-Dependent Electromechanics of Aqueous Liquids, Electrowetting and Dielectrophoresis," Langmuir, **20**, pp. 2813–2818.

[23] Walker, S. W., and Shapiro, B., 2006, "Modeling the Fluid Dynamics of Electrowetting on Dielectric (EWOD)," J. Microelectromech. Syst., **15**(4), pp. 986–1000.

[24] Singh, P., and Aubry, N., 2007, "Transport and Deformation of Droplets in a Microdevice Using Dielectrophoresis," Electrophoresis, **28**, pp. 644–657.

[25] Bahadur, V., and Garimella, S. V., 2006, "An Energy-Based Model for Electrowetting-Induced Droplet Actuation," J. Micromech. Microeng., **11**(8), pp. 1994–1503.

[26] Baird, E., Young, P., and Mohseni, K., 2007, "Electrostatic Force Calculation for an Ewod-Actuated Droplet," Microfluid. Nanofluid., **3**(6), pp. 635–644.

[27] Buehrle, J., Herminghaus, S., and Mugele, F., 2003, "Interface Profiles Near Three-Phase Contract Lines in Electric Fields," Phys. Rev. Lett., **91**(4), p.

208301.
[28] Kang, K. H., 2002, "How Electrostatic Fields Change Contact Angle in Electrowetting," Langmuir, **18**(26), pp. 10318–10322.
[29] Vallet, M., Vallade, M., and Berge, B., 1999, "Limiting Phenomena for the Spreading of Water on Polymer Films by Electrowetting," Eur. Phys. J. B, **11**(4), pp. 583–591.
[30] Jackson, J. D., 1998, *Classical Electrodynamics*, Wiley, New York.
[31] Landau, L. D., Lifshitz, E. M., and Pitaevskii, L. P., 1984, *Electrodynamics of Continuous Media*, 2nd ed., Pergamon, New York, Vol. 8.
[32] Saville, D. A., 1984, "Electrohydrodynamics: The Taylor–Melcher Leaky-Dielectric Model," Annu. Rev. Fluid Mech., **29**, pp. 27–64.
[33] For the electrostatic approximation to apply, the characteristic time scale for electric phenomena, $\tau = \epsilon = \sigma$ must be small. Note that τ is the ratio of dielectric permeability to conductivity of the medium. For the microfluidic applications considered here, this condition will usually be valid. For example, pure water has a electrical relaxation time of $\approx 10^{-4}$ and a hydrodynamic time scale of ≈ 0.045. See [45] for more details.
[34] Penfield, P. A., and Haus, H. A., 1967, *Electrodynamics of Moving Media*, MIT, Cambridge.
[35] Stratton, J. A., 1941, *Electromagnetic Theory*, McGraw-Hill, New York.
[36] Woodson, H. H., and Melcher, J. R., 1968, *Electromechanical Dynamics, Part I: Discrete Systems*, Wiley, New York.
[37] Bobbio, S., 2000, *Electrodynamics of Materials: Forces, Stresses, and Energies in Solids and Fluids*, Academic, New York.
[38] Melcher, J. R., 1981, *Continuum Mechanics*, MIT, Cambridge.
[39] Woodson, H. H., and Melcher, J. R., 1968, *Electromechanical Dynamics, Part II: Fields, Forces, and Motion*, Wiley, New York.
[40] Woodson, H. H., and Melcher, J. R., 1968, *Electromechanical Dynamics, Part III: Elastic and Fluid Media*, John, New York.
[41] Mohseni, K., and Baird, E., 2007, "A Unified Velocity Model for Digital Microfluidics," Nanoscale Microscale Thermophys. Eng., **11**(1&2), pp. 109–120.
[42] If the droplet is initially charged or if it is short cut to the electrodes on one side of the channel while isolated from the electrodes on the other side, there will be another source of force on the droplet represented locally by $\rho_f \mathbf{E}$. Our approach here can be easily extended to this case as well.
[43] Unless the droplet is isolated only from the electrodes on one side of the channel. In this case the droplet stays at the voltage of the electrodes on the other side of the channel.
[44] Holst, T. L., 1977, "Numerical Solution of Axisymmetric Boattail Flow Fields With Plume Simulators," *15th Aerospace Sciences Meeting and Exhibit*, Los Angeles, CA, Jan. 24–26, Paper No. AIAA 77-224.
[45] Melcher, J. R., and Taylor, G. I., 1969, "Electrohydrodynamics: A Review of the Role of Interfacial Shear Stresses," Annu. Rev. Fluid Mech., **1**, pp. 111–146.